Journal of Materials Science: Materials in Electronics (2019) 30:200–211
https://doi.org/10.1007/s10854-018-0282-8

Large electromechanical strain and electrostrictive effect in $(1-x)(Bi_{0.5}Na_{0.5}TiO_3–SrTiO_3)–xLiNbO_3$ ternary lead-free piezoelectric ceramics

Lei Wu[1] · Youbin Yang[1] · Shengju Zhu[1] · Bo Shen[1] · Querui Hu[2] · Jing Chen[2] · Ying Yang[2] · Yidong Xia[1] · Jiang Yin[1] · Zhiguo Liu[1]

Received: 10 July 2018 / Accepted: 23 October 2018 / Published online: 1 November 2018

Abstract
Lead-free $(1-x)(0.8Bi_{0.5}Na_{0.5}TiO_3–0.2SrTiO_3)–xLiNbO_3$ (BNST–*x*LN, $x=0$–0.08) piezoelectric ceramics were fabricated by a solid-state sintered technology. The effects of LN-doping on the structural and electrical properties of the BNST–*x*LN system were systematically investigated. The results of Raman spectroscopy revealed that the substitution of LN softens the phonon vibrations in the BNST–*x*LN system, in accordance with the remarkable reduction in the phase transition temperature (T_{F-R}), remnant polarization (P_r), negative strain (S_{neg}) and piezoelectric coefficient (d_{33}). However, the degradation of the long-range ferroelectric orders was accompanied by a significant increase in the electric field–induced strain response. At $x=0.04$, a maximum unipolar strain of ~0.36% with a corresponding normalized strain (S_{max}/E_{max}) of ~600 pm/V was obtained at room temperature, which should be mainly ascribed to the reversibly electric field-induced phase transition between the ergodic relaxor and ferroelectric phases due to their comparable free energies in the two-phase coexistence region. Moreover, it was also found that the BNST–*x*LN system processes predominant electrostrictive behaviors with relatively high electrostrictive coefficient (Q_{33}) and excellent temperature stability when the field-induced phase transition cannot be trigged by the applied electric field, as evidenced by a fact that the Q_{33} value of BNST–0.08LN ceramic keeps almost constant as high as ~0.028 m^4/C^2 in the temperature range from room temperature to 120 °C.

1 Introduction

Piezoelectric ceramics, which allow the inter-conversion between the electrical and mechanical energies, play an important role in various electronic devices such as actuators, sensors, transducers and ultrasonic motors, etc. In the past decades, the lead-based piezoelectric materials, such as $Pb(Zr,Ti)O_3$ (PZT) and $Pb(Mg_{1/3}Nb_{2/3})O_3$ (PMN), have been the most popular choice in the real-world applications due to their excellent piezoelectric and electromechanical properties. However, the severe environmental pollution caused by the toxicity of Pb has urged the extensive researches of competitive lead-free alternatives [1–4]. Recently, a sort of incipient piezoelectric ceramics featuring large electric field–induced strain response, represented by $0.92Bi_{0.5}Na_{0.5}TiO_3–0.06BaTiO_3–0.02K_{0.5}Na_{0.5}NbO_3$ (BNT–BT–KNN), have been considered as one of the most promising candidates to replace Pb-based materials in the actuator applications [5–7]. As noted that the emergence of the large usable strain in the BNT-based systems is accompanied by the poor piezoelectric coefficient (d_{33}), it was proposed that the incipient strain is not related to the domain switching in the normal ferroelectrics just as PZT, but should be ascribed to the "nonpolar" or ergodic relaxor phase that can be transformed into a metastable ferroelectric state under external electric field [8, 9]. This hypothetical mechanism has been well confirmed by a series of studies of in-situ X-ray diffraction (XRD) and transmission electron microscopic (TEM) for the BNT-based incipient piezoelectrics, where a reversible phase transformation between metrically cubic and noncubic phases was observed under the electric field [10–13].

Although the actuator performance of BNT-based incipient piezoelectric ceramics is comparable with that

✉ Jiang Yin
jyinnju@163.com

[1] National Laboratory of Solid State Microstructures, College of Engineering and Applied Sciences, Nanjing University, Nanjing 210093, China

[2] Department of State Key Laboratory of Mechanics and Control of Mechanical Structures, Nanjing University of Aeronautics and Astronautics, Nanjing 210016, China

of Pb-based ones, several drawbacks have been identified to hinder the practical application of this sort of materials. According to the mechanism mentioned above, the incipient piezoelectric strain cannot be activated unless the applied electric field is large enough to overcome the energy barrier between the initial ergodic relaxor phase and the field-induced ferroelectric phase; consequently, a large hysteresis is not avoidable in the electric field-dependent strain curve. In addition, the threshold electric field for the incipient piezoelectric properties enhances significantly when the temperature is increased, thus, resulting in a relatively poor temperature stability of the polarization and strain responses [7, 14]. To resolve these two problems, one of the possible solutions is to utilize the electrostriction of the BNT-based incipient piezoelectric ceramics while suppressing the reversible relaxor-to-ferroelectric phase transition. Compared with the incipient piezoelectric behaviors, the electrostrictive strain derived from the intrinsic lattice deformation of relaxor ferroelectrics has special merits of little hysteresis and prominent temperature stability, which is in favor of the applications requiring high-frequency operation, precise position control and quick response time [15, 16]. Zhang et al. found that the BNT–BT–KNN electrostrictors evolved from the incipient piezoelectric composition can keep relatively large electrostrictive coefficients (Q_{33}) in a wide temperature range, which is even higher than that of some lead-containing relaxor ferroelectrics [17, 18]. Similar phenomenon has also been achieved in many other BNT-based solid solutions such as $Bi_{0.5}Na_{0.5}TiO_3$–$BaTiO_3$–$(Sr_{0.7}Bi_{0.2})TiO_3$ [19], $Bi_{0.5}Na_{0.5}TiO_3$–$BaTiO_3$–$SrTiO_3$[20],$Bi_{0.5}Na_{0.5}TiO_3$–$Bi_{0.5}K_{0.5}TiO_3$–$KNbO_3$ [21], $Bi_{0.5}(Na_{0.82}K_{0.18})_{0.5}(Ti_{1-x}Sn_x)O_3$ [22], etc.

In general, to obtain large electromechanical strain or high electrostrictive coefficient in the BNT-based systems, the morphotropic phase boundary (MPB, between rhombohedral and tetragonal ferroelectric phases) compositions of BNT–BT or BNT–BKT are mostly chosen as matrix materials because of their promising ferroelectric and piezoelectric properties [5, 17–24]. However, some inspiring achievements have also been obtained in the BNT-based incipient piezoelectrics or electrostrictors developed by the specific compositions with polymorphic phase boundary (PPB) between rhombohedral ferroelectric and pseudo-cubic relaxor phase [25–31]. Tong et al. achieved an excellent normalized strain (S_{max}/E_{max}) above 850 pm/V in the ($Bi_{0.5}Na_{0.5}TiO_3$–$SrTiO_3$)–$NaNbO_3$ ceramics [29]. Cho et al. investigated the Fe-modified $Bi_{0.5}Na_{0.5}TiO_3$–$SrTiO_3$ system and found that the introduction of Fe can effectively improve the S_{max}/E_{max} of $Bi_{0.5}Na_{0.5}TiO_3$–$SrTiO_3$ ceramics over 500 pm/V at an ultra-low driving field of 20 kV/cm [30]. Bai et al. found that the BNT–$KNbO_3$–$SrTiO_3$ system exhibits not only a large strain of 0.34% with $S_{max}/E_{max}=486$ pm/V but also a high Q_{33} of ~ 0.024 m^4/C^2 [31]. It is noted that the PPB composition $Bi_{0.5}Na_{0.5}TiO_3$–$0.2SrTiO_3$ (BNST) binary solid solutions have preferable ferroelectric and piezoelectric characteristics [26]. On the other hand, $LiNbO_3$ (LN), which is one of the ABO_3-type ferroelectrics with a rhombohedral symmetry, has been well identified to be an efficient chemical modifier to improve the electrical properties in BNT-based systems [32–36]. Compared with other perovskite dopants such as $K_{0.5}Na_{0.5}NbO_3$, $NaNbO_3$ or $SrTiO_3$, $LiNbO_3$ has a smaller cation (Li^+) at the A site. Chen et al. found that $LiNbO_3$ incorporation in the BNT–6BT lattices not only causes a compositionally induced ferroelectric-to-relaxor phase transition with the decreased phase transition temperatures, but also creates a special crystalline distortion with core–shell nano-domains, resulting in a giant electromechanical strain of ~ 0.6% at 70 kV/cm [32]. Therefore, it is reasonable to assume that combining BNST as a host material and LN as a dopant could be an effective way to obtain promising lead-free piezoelectrics and electrostrictors. In this study, a new BNST–*x*LN ternary piezoelectric ceramics were synthesized by using a conventional solid-state reaction method, and their phase structure, dielectric, ferroelectric, electromechanical and electrostrictive properties were investigated in detail.

2 Experimental

Lead free $(1-x)(0.8Bi_{0.5}Na_{0.5}TiO_3$–$0.2SrTiO_3)$–$xLiNbO_3$ (BNST–*x*LN, $x=0$–0.08) piezoelectric ceramics were prepared by a conventional solid-state reaction method using powders of Bi_2O_3 (99.9%), TiO_2 (99.6%), Nb_2O_5 (99.9%), Na_2CO_3 (99.5%), Li_2CO_3 (99.9%) and $SrCO_3$ (99%) as raw materials. For each composition, the raw materials were weighed according to the stoichiometric formula. The mixed powders were ball-milled in ethanol for 24 h. The dried slurries were calcined in covered alumina crucibles at 850 °C for 2 h and then ball-milled again for 24 h. After mixed with polyvinyl alcohol (PVA) as a binder for granulation, the precursors were subsequently pressed into disk pallets with a diameter of 10 mm under 160 MPa. Sintering of BNST–*x*LN ceramics was carried out at 1050–1150 °C depending on the LN content. To minimize the evaporation of the volatile elements Bi, Na and Li, the disks were embedded in the corresponding powders during sintering.

The crystal structures of the ceramics were characterized by using powder X-ray diffraction (XRD, Rigaku Ultima III, Japan). The microstructures of the thermally etched samples were observed by using scanning electron microscopy (SEM, XL30 Philips). Raman spectra of the polished sintered ceramics were recorded by using 538-nm excitation with a Jobin-Yvon LabRam HR800 (Horiba JobinYvon Inc., Paris, France). For the electrical measurements, the sintered ceramics were polished and coated with silver paste on both surfaces, and then fired at 650 °C. The ferroelectric

properties and electric field–induced strain behaviors were measured at 1 Hz by using a ferroelectric test unit (Precision Premier II and TF-2000, Radiant Tech, USA) in a silicon oil bath under the controllable temperature. After the samples were poled sufficiently, the temperature-dependent dielectric constant and loss tangent of the poled samples were measured by using an impedance analyzer (HP 4294A, Hewlett, Packard) at frequencies ranging from 1 kHz to 1 MHz. The piezoelectric coefficient (d_{33}) was tested by using a Berlincourt d_{33} meter (ZJ–6 A, Chinese Academic Society, China).

3 Results and discussion

Figure 1 shows the XRD patterns of the unpoled BNST–*x*LN ceramics with different LN content ($x = 0$–0.08) at room temperature. All the samples exhibit a pure perovskite structure with no secondary phase, suggesting that the dopant LN has successfully diffused into the BNST lattices and complete a solid solution. According to the presence of the unsplit (1 1 1) ($2\theta = \sim 40°$) and (2 0 0) ($2\theta = \sim 46.5°$) reflection peaks as shown in Fig. 1b, c, it can be identified that the phase structure of the BNST–*x*LN system has the feature of pseudo-cubic symmetry. No obvious change in the peak positions and intensity depending on the composition was detected. This sort of pseudo-cubic symmetry displayed in Fig. 1 has been commonly observed in the unpoled BNT-based relaxor ferroelectrics. The formation of the single (1 1 1) and (2 0 0) peaks should be ascribed to the overlapping of the nanoscale domains with non-cubic distortion, as evidenced by the appearance of 1/2{ooe}- and 1/2{ooo}-type superstructure reflections in the TEM diffraction patterns. However, the size base on the superlattice refections was estimated to be less than 10 nm, which is beyond the detection limit of conventional XRD techniques [11, 37]. Considering the close similarities between the BNST–*x*LN and other BNT-based solid solutions, it might be reasonable to assume that the non-cubic domains in this investigated system should only exist as polar nanoregions (*PNR*s), but which could transform into a long-range ferroelectric phase under external electric filed either permanently or temporarily depending on the LN content [8].

Figure 2 exhibits the SEM micrographs of the polished and thermally etched BNST–*x*LN ceramics with different LN content. All the samples display well homogeneous and highly dense microstructure with clear grain boundary. It can be found that both geometric profile and average size of the crystalline grains are influenced by the doping of LN slightly. As the doping ratio increases, the grain morphology changes into more regular round shape, as well as the average size decreases from ~ 1.9 μm for $x = 0$ to ~ 1.3 μm for $x = 0.08$. The results are consistent with a previous report on LN-doped $(Bi_{0.5}Na_{0.5})TiO_3$–$(Ba_{0.7}Ca_{0.3})TiO_3$ ceramics, which may be attributed to the reduction of the oxygen vacancy concentrations induced by the donor doping at the B site (Nb^{5+} substitutes for Ti^{4+}) [36].

To further confirm the compositionally induced phase transition behaviors of the BNST–*x*LN system, Raman spectroscopy, which can probe lattice vibrations directly in a local ionic configuration, was utilized in this work. Figure 3a shows the room-temperature Raman spectra for the BNST–*x*LN ceramics with different amount of LN from 100 to 1000 cm^{-1}. It is clear that the overall signature of the spectra performs a relatively broad and diffuse characteristic just as other BNT-based solid solutions, which can be divided into four main regions: (i) the modes of wavenumbers ≤ 200 cm^{-1} related to A-site vibrations of the perovskite structure; (ii) the modes around 260 cm^{-1} associated with B–O vibrations; (iii) the 450–700 cm^{-1} host modes assigned to the vibration of the BO_6 octahedra; (iv) the high-frequency modes above 700 cm^{-1} modes related to Al (longitudinal optical) and E (longitudinal optical) overlapping

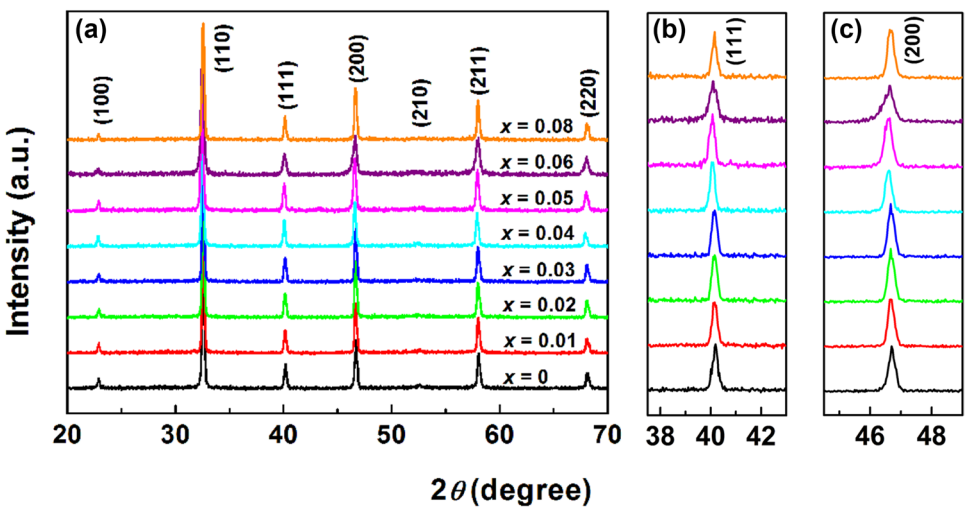

Fig. 1 XRD patterns of the BNST–*x*LN system with different LN content in the 2θ range of **a** 20°–70°, **b** 37.5°–43° and **c** 44.5°–49°

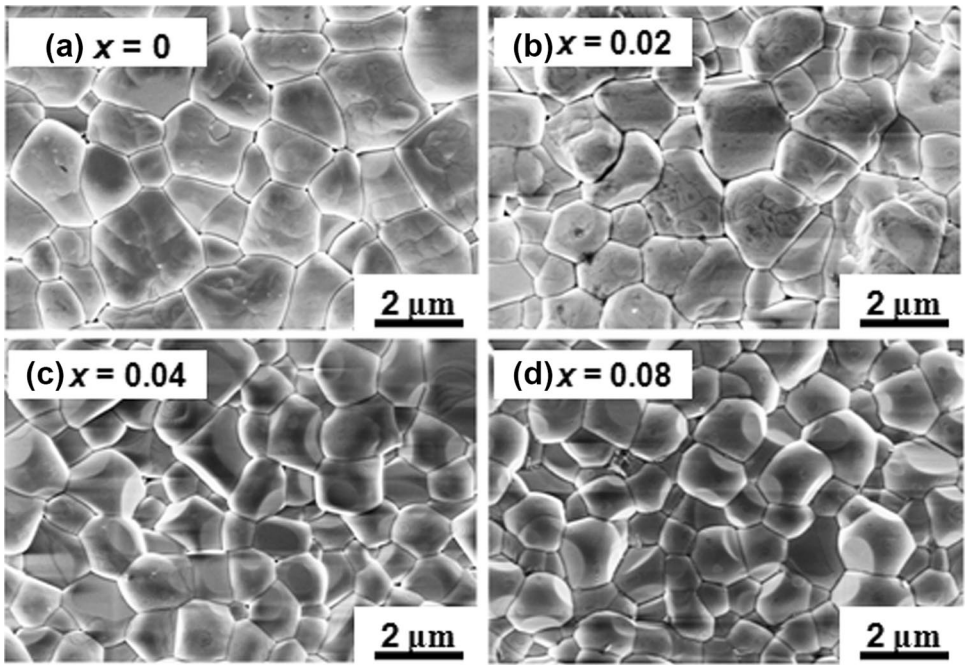

Fig. 2 SEM morphologies of the polished and thermally etched BNTST–*x*LN samples with **a** $x=0$; **b** $x=0.02$; **c** $x=0.04$ and **d** $x=0.08$

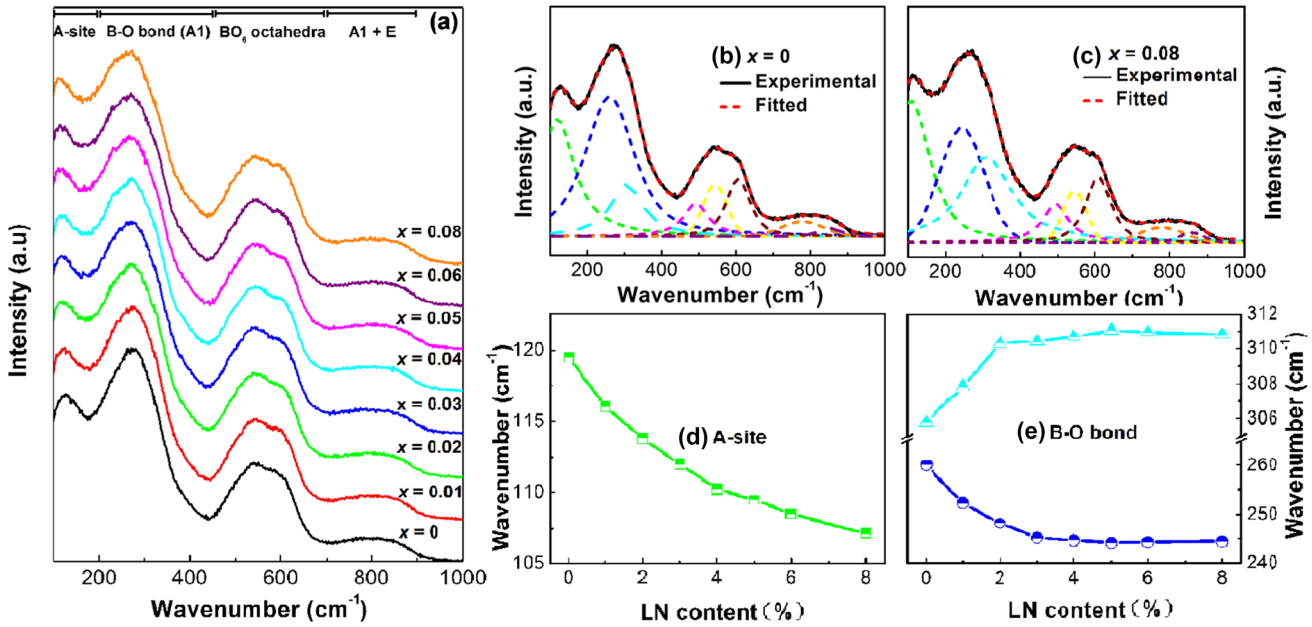

Fig. 3 **a** Raman spectrum for the BNST–*x*LN ceramics with different LN content; spectra deconvolution of **b** the unmodified BNST ceramic and **c** the BNST–0.08LN ceramic at room tempature performed by eight Gaussian–Lorentzian modes. The composition-dependence of the position of Raman vibrational modes with **d** A-site and **e** B–O bond, respectively

bands [38]. Based on the previous literatures, the spectra were well fitted by the Gaussian–Lorentzian function with a collection of eight curves [33, 39], as shown in Fig. 3b, c. In order to quantify the modes variations, the peak positions of the fitting bands corresponding to A-site and B–O vibrations as a function of LN content are plotted in Fig. 3d, e, respectively. Although the BNST–*x*LN ceramics appear to be the similar pseudo-cubic phase in a large length-scale with little composition-dependence, the particular phonon behavior reflected by the spectra demonstrates a rhombohedral and tetragonal mixed-phase nature of the average cubic structure, which is evidenced by the two distinct splitting bands in the mode corresponding to B–O vibrations centered around 260 cm^{-1} [19, 40]. Moreover, the A-site band

shifts to low wavenumbers gradually with the increase in LN content, indicating a weakening of the bonding between the A-site cations and oxygen probably due to the loss of orbital hybridization between the $6s^2$ orbitals of Bi^{3+} and the oxygen *p* orbitals. It is proposed that the Bi lone pair interacting with the oxyen octahedra can be conductive to develop *PNR*s with relaxor behaviors in the BNT-based systems [41]. In addition, the two distinct bands associated with the vibrations of the B–O bond shift apart from each other as the doping amount increases, leading to a steady softening of the phonon vibrations when $x \geq 0.03$. Since the vibrations of the B–O bonds are closely related to the dynamics of *PNR*s, the steady phonon softening occurred around $x = 0.03$ illustrates an emergence of the macroscopic relaxor characteristics in the samples with the increased octahedral distortion [42]. Combined with other studies on the Raman data of BNT-based systems, it is rationalized to draw a conclusion that this abrupt change implies a ferroelectric-to-relaxor phase transition, and the BNST–*x*LN ceramics should favor the pseudo-cubic relaxor phase at high LN content ($x \geq 0.03$).

Figure 4a shows the temperature-dependent dielectric constant and loss tangent of the unmodified BNST ceramic at various frequencies as a representative for the BNST–*x*LN system, and the temperature-dependence of relative permittivity and loss tangent for the poled BNST–*x*LN samples with different LN content measured at the frequency of 1 kHz is shown in Fig. 4b. It is obvious that the dielectric curves of the poled BNST–*x*LN ceramics exhibit strong frequency dispersion and two distinctive anomalies in the measured temperature range, which should be attributed to the thermal evolution of *PNR*s. The former anomaly T_{F-R} at lower temperatures is always considered to be associated with the evolution of the initially coexisting rhombohedral and tetragonal *PNR*s, where the ferroelectric-to-relaxor phase transition occurs. The latter one at higher temperatures is marked as T_m where the dielectric constant reaches the maximum value, corresponding to the relaxation of tetragonal symmetry *PNR*s emerged from rhombohedral *PNR*s [43, 44]. The base composition $x = 0$ was found to have a relatively frequency-independent T_{F-R} peak both in the dielectric constant and loss tangent curves at temperature ~ 62 °C. The change in the frequency-dependent dispersion observed around T_{F-R} suggests that a low-temperature frozen *PNR*s with strong correlation [non-ergodic relaxor (*NR*) state, which can be converted irreversibly into a stable ferroelectric order by sufficiently large electric field] transform into a high-temperature flexible *PNR*s with dynamical activity [ergodic relaxor (*ER*) state] upon heating [9, 34]. With the increase of LN content, the T_{F-R} value decreases monotonously and the corresponding peak becomes ambiguous progressively. When $x \geq 0.02$, no distinctive T_{F-R} peak can be accurately defined in the dielectric curves, implying that the

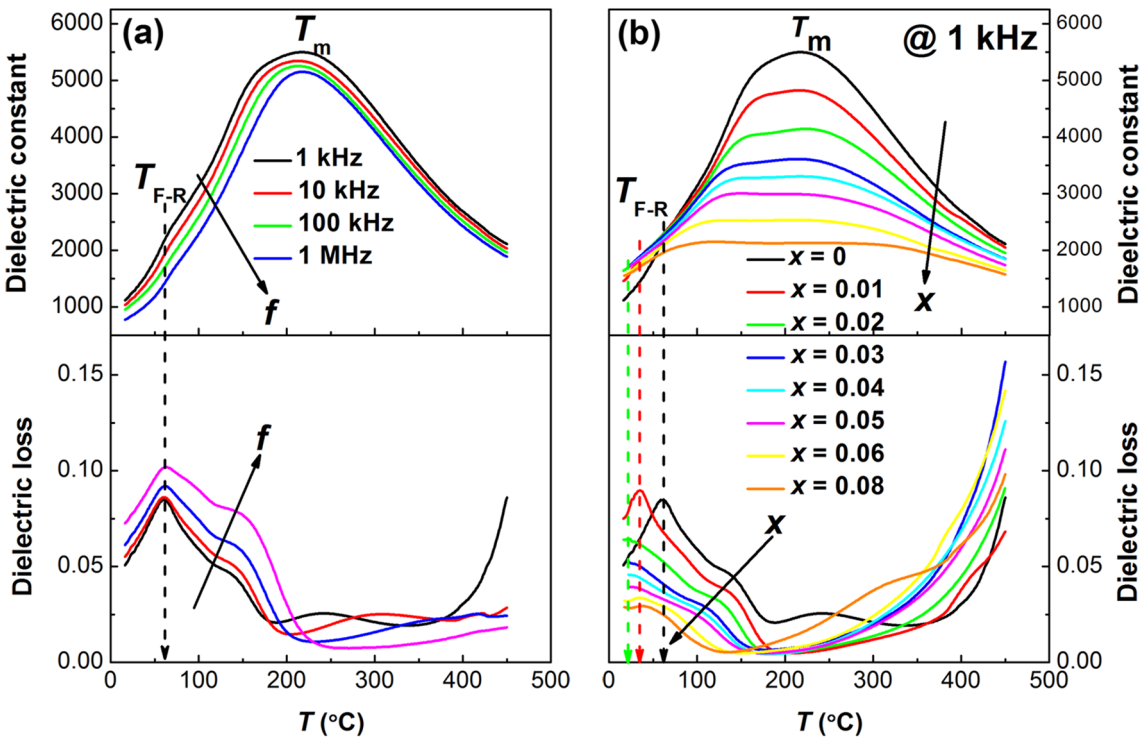

Fig. 4 The temperature-dependence of the dielectric constant and loss tangent for the poled **a** BNST ceramic under the frequency from 1 kHz to 1 MHz and **b** BNST–*x*LN ceramics with different LN content at 1 kHz

T_{F-R} of the samples with high LN concentrations ($x \geq 0.02$) locates around or below room temperature. The absence of T_{F-R} indicates that these compositions are *ER* state at room temperature, which would transform to a ferroelectric phase under electric field but come back to the initial state once the applied electric field is removed. On the other hand, it can be seen that the doping of LN has another effect to broaden the T_m anomalies gradually and decrease the dielectric constant at T_m significantly, which should be ascribed to the enhanced disordered distribution both in A- and B-sites induced by the LN-modification. As a result, the BNST–0.08LN ceramic presents a rather flat dielectric constant curve with variation less than ± 10% (taking 150 °C as a reference point) ranging from 55 to 370 °C at 1 kHz. Meanwhile, its loss maintains below 0.1 from room temperature up to 450 °C. These features predict that the sample with $x = 0.08$ may be suitable for the high temperature capacitor applications.

Figure 5a shows the room-temperature polarization hysteresis (*P*–*E*) loops for the BNST–*x*LN ceramics under an electric field of 60 kV/cm, and the variation in maximum polarization (P_m), remnant polarization (P_r) and coercive field (E_c) with respect to the LN content is plotted in Fig. 5b.

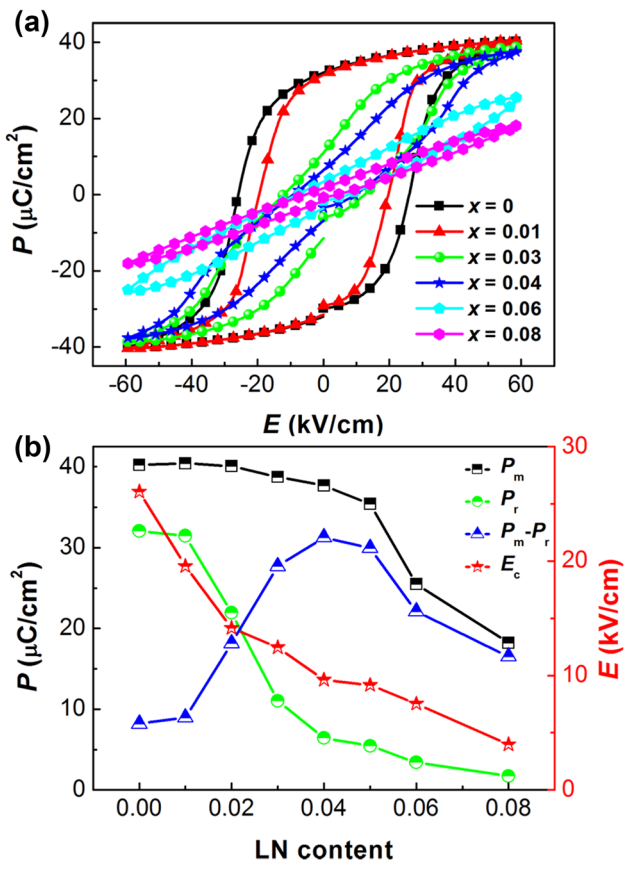

Fig. 5 **a** *P*–*E* hysteresis loops and **b** the ferroelectric properties (P_m, P_r, P_m–P_r and E_c) of BNST–*x*LN ceramics with different LN content at room temperature

The base composition BNST without any LN substitution and the sample with $x = 0.01$ exhibit well-saturated *P*–*E* loops with relatively large P_r and E_c as typical ferroelectrics, consisting with their T_{F-R} value located above room temperature. It can be found that the further addition of LN decreases both P_r and E_c drastically while having less influence on the P_m value; consequently, resulting in the appearance of pinched *P*–*E* loops around $x = 0.04$. The significant reduction in P_r and E_c indicates that the long-range ferroelectric order in the BNST ceramic is disrupted and transformed into the non-polar or the ergodic relaxor phase by the LN-modification, however, the slight change in P_m reveals a fact that the ergodic relaxor phase can convert into a long-rang ferroelectric state under an external electric field due to the comparable free energies between the two phases [8, 9]. In addition, it is noted that the electric field-induced phase transition is apparently decayed when $x \geq 0.06$, which is evidenced by the presence of the slim loops with relatively small P_m.

The compositionally induced ferroelectric-to-ergodic relaxor phase transition can also be well verified by the bipolar electrical-field–induced strain (*S*–*E*) curves, as shown in Fig. 6a, c presents the evolution in negative strain (S_{neg}) and positive strain (S_{pos}) as a function of the LN content. The unmodified BNST ceramic displays a typical ferroelectric feature characterized by the butterfly-shaped bipolar *S*–*E* curve with a visible S_{neg} of ~ 0.064%. The S_{neg} that is closely related to the domain back switching during the bipolar cycle loading was found to first increase to a maximum value of ~ 0.094% at $x = 0.01$, possibly due to the enhanced domain wall density and mobility with the decreased E_c [34]. However, a sharp reduction in S_{neg} is accompanied by a concurrent enhancement in S_{pos} with the further increase in LN content. When $x \geq 0.03$, the bipolar *S*–*E* loops transform into the sprout-shaped ones, indicating a drastic deviation from the typical ferroelectric behavior owing to the disappearance of S_{neg}. For the critical composition $x = 0.04$, a maximum S_{pos} value of ~ 0.35% together with a negligible S_{neg} were obtained during bipolar loading, which are mainly attributed to the formation and stabilization of the ergodic relaxor phase in the BNST–*x*LN system, in accordance with the polarization measurement.

Figure 6b shows the room-temperature unipolar strain response of the BNST–*x*LN ceramics measured at an applied field of 60 kV/cm. The pure BNST ceramic exhibits a quasi-linear unipolar *S*–*E* curve with a strain response of ~ 0.16% at 60 kV/cm, which is typical for the ferroelectric materials. With the introduction of LN, the unipolar strain level increases slightly to ~ 0.17% for the composition $x = 0.01$, and then abruptly to a top value of ~ 0.36% when LN content reaches 0.04. Note that this large strain achieved in the unipolar *S*–*E* curve is accompanied by a pronouncedly hysteretic behavior, indicating that the origin of the large strain

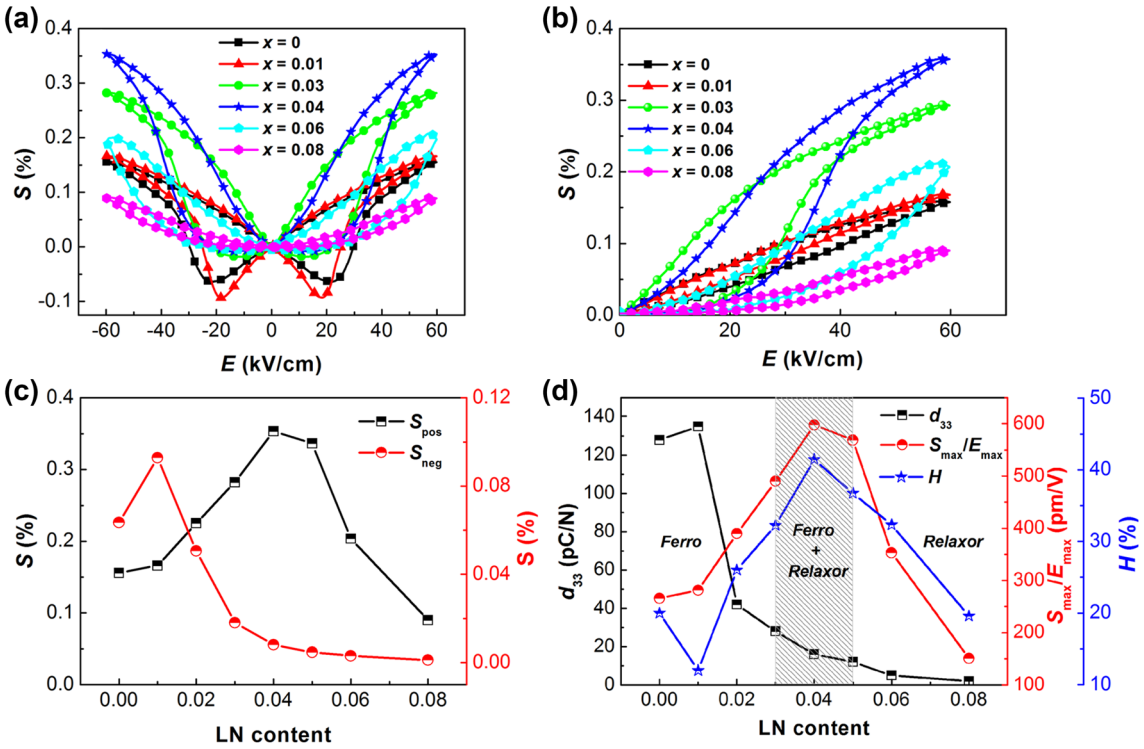

Fig. 6 The composition-dependent **a** bipolar and **b** unipolar *S*–*E* curves of BNST–*x*LN ceramics under electric field of 60 kV/cm; the variation of **c** S_{pos}, S_{neg} and **d** S_{max}/E_{max}, d_{33} and H with respect to LN content at room temperature

response is different from the converse piezoelectric effect in ferroelectrics.

To further clarify the mechanism of the strain response in this studied system, a summary of the piezoelectric coefficient (d_{33}), the normalized strain (S_{max}/E_{max}) and the hysteresis ($H = \Delta S/S_{max}$) (ΔS is the difference between the two strain values at $E_{max}/2$) with respect to the LN content is presented in Fig. 6d, where different phase zones can be roughly marked. For the base composition BNST, a S_{max}/E_{max} of ~ 266 pm/V was calculated from the quasi-linear unipolar *S*–*E* curve, which should be mainly derived from the variation in the lattice distortion induced by the converse piezoelectric effect and the domain reorientation process under the applied electric field as evidenced by the relatively large d_{33} of ~ 128 pC/N. At $x = 0.01$, both d_{33} and S_{max}/E_{max} increase to ~ 135 pC/N and ~ 281 pm/V, respectively. The slight increase in the piezoelectricity may be ascribed to a relatively low energy barrier for the polarization switching provided by the phase coexistence with nano-domains [45]. However, the composition-dependent behavior of the quasi-static piezoelectric properties shows an obviously different variation tendency from that of the dynamic large-signal strain performances with the further incorporation of LN. The d_{33} value decreases remarkably to ~ 42 pC/N at $x = 0.02$, and then gradually approaches to ~ 2 pC/N at $x = 0.08$, while a sudden jump in the S_{max}/E_{max} value was noted for the compositions in the vicinity of $x = 0.04$. It is clear that the maximum S_{max}/E_{max} value of ~ 600 pm/V in the BNST–0.04LN ceramic is no longer dominated by the contributions of the true piezoelectric response and the irreversible domain switching because of the poor d_{33} of ~ 16 pC/N, but should be mainly originated from the extrinsic effects of a crossover from a dominant ferroelectric (*FE*) or nonergodic relaxor (*NE*) phase to a dominant ergodic relaxor (*ER*) phase. Around the two-phase coexisted region, the reversibly ergodic relaxor-to-ferroelectric phase transition can easily take place under the external electric field, which is reflected by the considerably large hysteresis in the non-linear unipolar *S*–*E* curve, resulting in the large strain response. Moreover, the dramatic reduction in S_{max}/E_{max} at high LN contents ($x \geq 0.06$) confirms that the ferroelectric and relaxor phases only have the competitive free energy in a narrow composition range, and the field-induced long-range state cannot be established in the samples with $x \geq 0.06$ throughout the range of applied field as investigated. It is noted that the critical composition $x = 0.04$ in our case exhibits a large S_{max}/E_{max} of ~ 600 pm/V at a moderate electric field of 60 kV/cm with a relatively low hysteresis of ~ 41%. Hence, it can be concluded that the combination of BNST as a matrix material and LN as a chemical modifier is effective to enhance the actuating performances.

On the other hand, a typical electrostrictive behavior was also observed in the BNST–0.08LN ceramic as evidenced by the weakened hysteretic behaviors in both *P*–*E* and *S*–*E* loops. For the electrostrictive materials, the sign of the electric field-induced deformation is independent on the polarity of the field and proportional to the square of the applied electric field, as given by $S = QP^2$, where the electrostrictive coefficient (Q) is the most crucial parameter of the electrostrictive properties. It is known that a comparatively large electrostriction can be obtained at ambient temperature in the relaxor ferroelectrics if the phase transition temperature is close to room temperature. Meanwhile, the magnitude of Q has been reported to have a correlation with the amplitude of the excitation electric field. To evaluate the suitability of the BNST–*x*ST ceramics for the actual application as electrostrictors, the electrostrictive behaviors under different external electric field for the samples with negligible S_{neg} ($x = 0.04$–0.08) were depicted in Fig. 7a–c, in which the values of Q_{33} were determined from the slope of S–P^2. It is disclosed that the critical composition $x = 0.04$ exhibits the

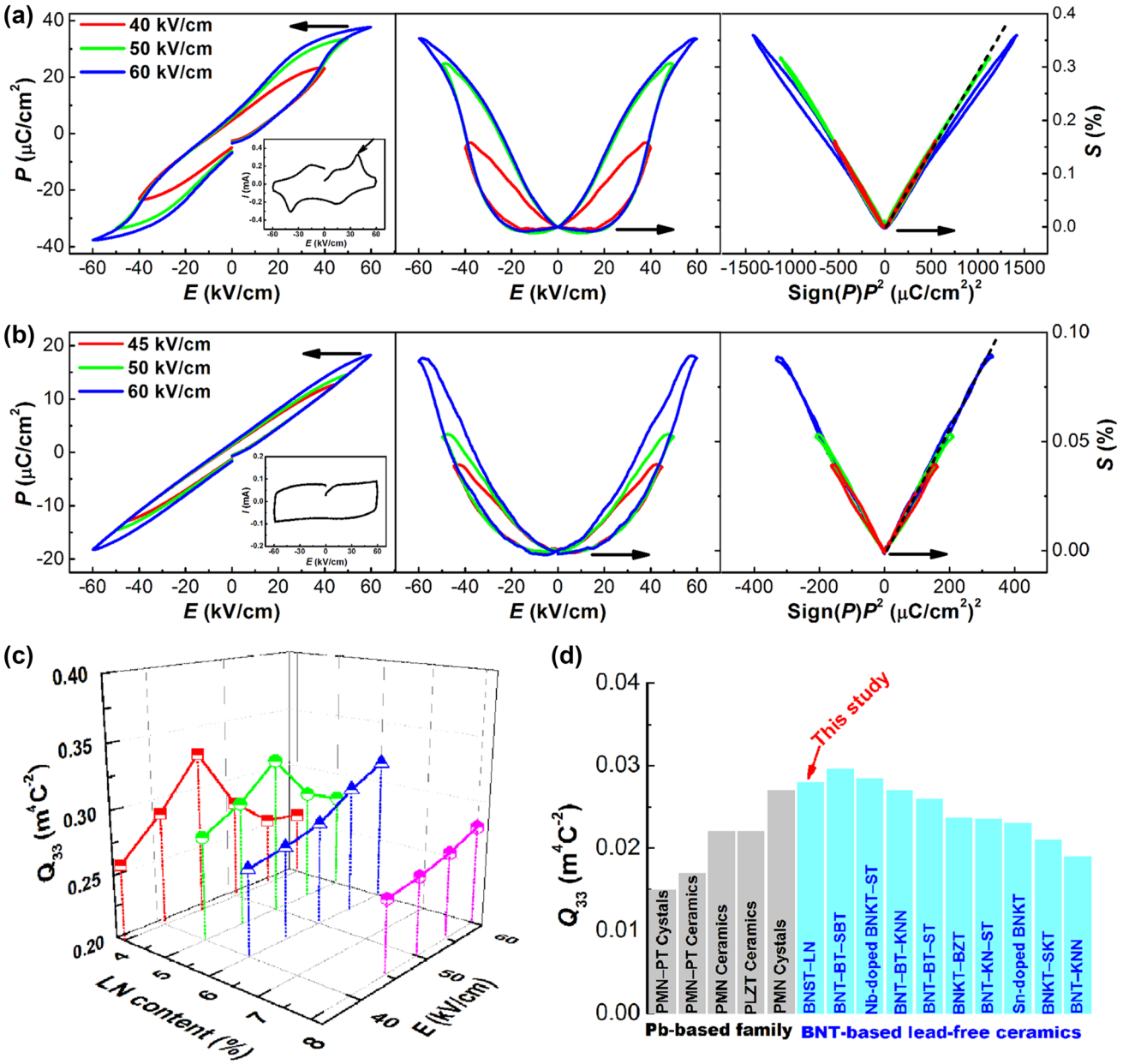

Fig. 7 *P*–*E* loops, bipolar *S*–*E* curves and *S*–P^2 plots under different electric fields for the samples with **a** $x = 0.04$ and **b** $x = 0.08$ (insets of **a** and **b** are the *J*–*E* curves for the indicated compositions), respectively; **c** the Q_{33} value of the BNST–*x*LN ceramics with $x = 0.04$–0.08 as functions of the amplitude of electric field; **d** a summary of the Q_{33} of representative lead-based and BNT-based electrostrictive materials compared with that of the BNST–0.08LN specimen

thin elliptical *P*–*E* loops and parabolic bipolar *S*–*E* curves at low electric fields ($E \leq 40$ kV/cm) just as relaxor ferroelectrics. The linear relationship between the strain and the polarization square points out that the strain response below 40 kV/cm should be mainly derived from the electrostriction. However, both the polarization and strain curves appear to be saturated (denoted by the bends in the *P*–*E* and *S*–*E* hysteresis loops) with a steed increase in the hysteresis when the magnitude of external electric field increases beyond 50 kV/cm, leading to an apparent deviation from the linearity in the S–P^2 profiles. This result demonstrates the existence of other electromechanical coupling behaviors besides electrostriction at high electric fields ($E \geq 50$ kV/cm), such as local volume change originated from field-induced relaxor-to-ferroelectric switching. Sapper el al. proposed that the magnitude of the external electric field is crucial important to determine the stable phase regions of the BNT-based ergodic relaxors. The density and mobility of polar entities in the virgin relaxor state is strengthened by the linearly ramped electric field, and a first-order phase transition from the short-range relaxor state to the long-range ferroelectric order occurs when the applied field reaches the threshold field [which can be deduced from the current density–electric field (*J*–*E*) profiles such as the inset in Fig. 7a] [46]. As disclosed by the *J*–*E* curves, the field level required for trigging the phase transition increases from ~ 40 kV/cm for BNST–0.04LN to ~ 60 kV/cm for BNST–0.06LN gradually. It is noteworthy that the BNST–*x*LN ceramics with $x = 0.04$–0.06 show the similar variation in Q_{33} with respect to the amplitude of the applied field, featuring relatively large Q_{33} value (0.03–0.033 m^4/C^2) near the field-induced phase transition boundary.

In contrast, the strain response of the BNST–0.08 ceramic keeps the strongly linear dependence on polarization square in the electric field range of 45–60 kV/cm, which is consistent with no peak observed in the current switching. By increasing electric field, the measured Q_{33} value for the sample with $x = 0.08$ increases from ~ 0.026 m^4/C^2 at 45 kV/cm to ~ 0.028 m^4/C^2 at 60 kV/cm slightly, possibly due to the suppression of micro-domain reorientation at high electric fields [47]. The achievable Q_{33} value of this phenomenological electrostrictive mode is comparable with that of other BNT-based electrostrictive ceramics, and is higher than that of some lead-containing electrostrictors [16–22, 47–49], indicating that this investigated system also has great potential in the fabrication of lead-free electrostrictors.

For real-world applications of piezoelectric ceramics, temperature stability of the functional properties is as important as the other physical properties. Figures 8 and 9 display the temperature-dependent *P*–*E*/*J*–*E* loops,

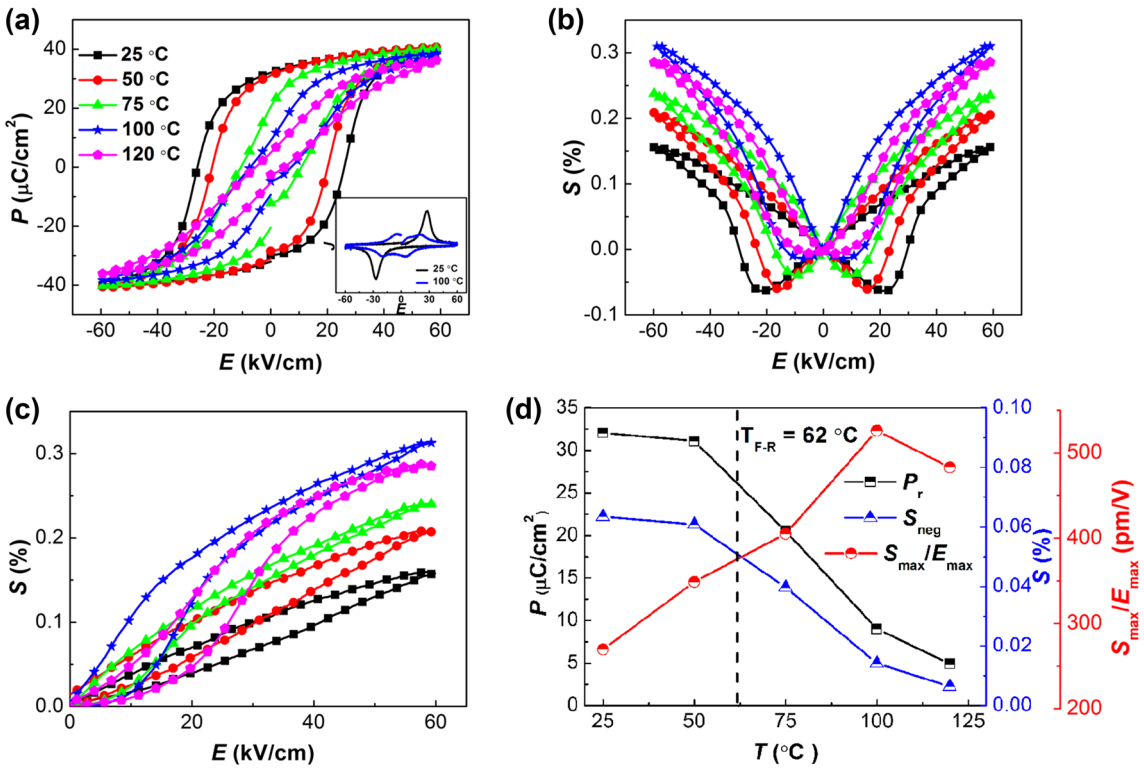

Fig. 8 The temperature dependence of **a** *P*–*E*/*J*–*E* loops, **b** bipolar and **c** unipolar *S*–*E* curves for the unmodified BNST ceramic; **d** the P_r, S_{neg} and S_{max}/E_{max}, of the BNST ceramic as functions of temperature

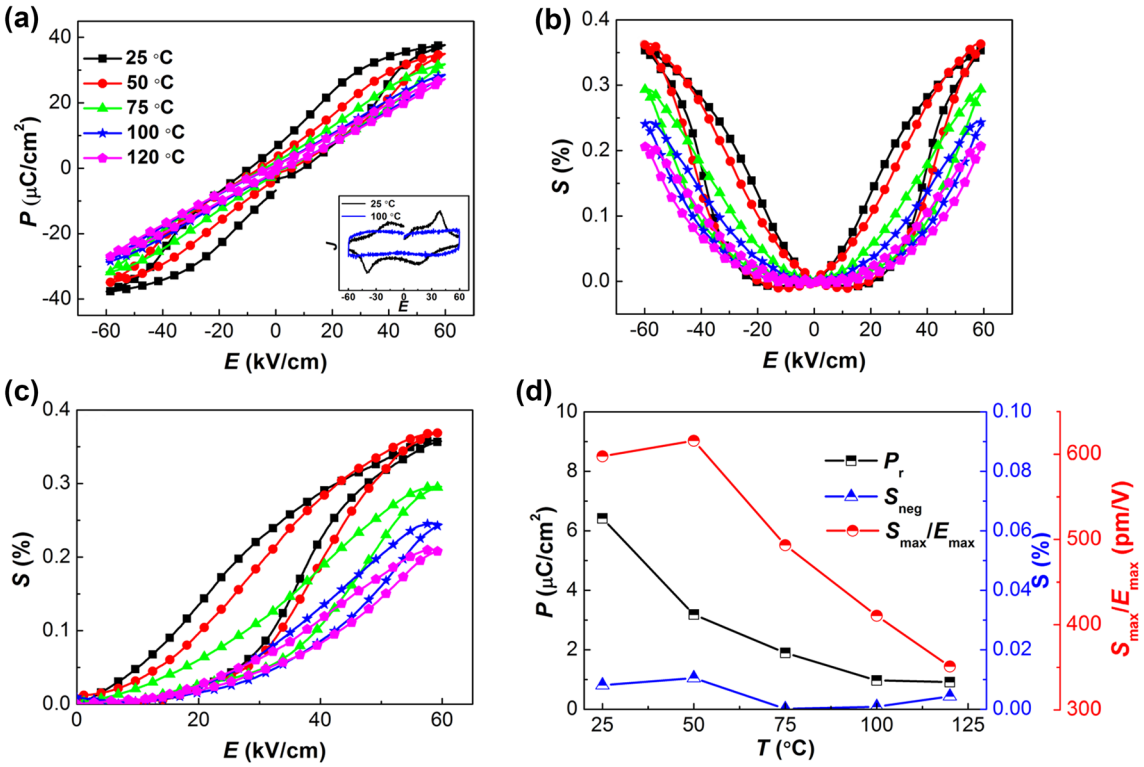

Fig. 9 The temperature dependence of **a** *P–E*/*J–E* loops, **b** bipolar and **c** unipolar *S–E* curves for the BNST–0.04LN ceramic; **d** the P_r, S_{neg} and S_{max}/E_{max}, of the BNST–0.04 ceramic as functions of temperature

bipolar and unipolar *S–E* curves measured under 60 kV/cm for the two representative compositions $x = 0$ and $x = 0.04$, respectively. For the unmodified BNST ceramic, which is a typical ferroelectrics at room temperature, it is obvious that the increased temperature affects the polarization and strain responses drastically. When the temperature extends above the determined T_{F-R} (~ 62 °C), the well saturated *P–E* hysteresis loops below 50 °C abruptly change into the constricted ones, coinciding with a deformation from the butterfly shape to the sprout shape in the bipolar *S–E* curves. Correspondingly, the normalized strain (S_{max}/E_{max}) calculated from the unipolar *S–E* curves firstly increases from ~ 266 pm/V at 25 °C to ~ 400 pm/V at 75 °C gradually, followed by a sudden increase to ~ 523 pm/V at 100 °C. However, at the further elevated temperature of 120 °C, the value of S_{max}/E_{max} drops to ~ 477 pm/V. The significant reduction in P_r and S_{neg} indicates that the long-range ferroelectric order at room temperature transforms to a relaxor state with short-range *PNR*s during heating. The temperature-induced phase transition is also well confirmed by the splitting of the current peaks in the *J–E* curves as shown in Fig. 8a. In addition, the pinched *P–E* loops and the sharply increased usable strain observed near T_{F-R} should be attributed to the nature of the ergodic relaxor phase, in which the dynamically active *PNR*s can be reversibly transformed into the ferroelectric macrodomains under a sufficiently large electric field.

In contrast, in the case of the critical composition $x = 0.04$, the thermal evolutions of the *P–E* and *S–E* loops exhibit a distinctly different behavior from that of the base composition BNST. Since the BNST–0.04LN ceramic is an ergodic relaxor featuring the pinched *P–E* loop and sprout-shaped bipolar *S–E* curve at room temperature, no remarkable changes in both P_r and S_{neg} were observed with the increase in temperature. However, the other characteristic values including P_m, S_{pos} and *H* decrease steadily when the temperature extends above 50 °C, suggesting that the increasing temperature enhances the random fields of the unfrozen *PNR*s continuously. We can speculate that the applied field of 60 kV/cm is no longer large enough to trigger the field-induced relaxor-to-ferroelectric phase transition at high temperatures ($T \geq 100$ °C) because no domain switching take place, as evidenced by the disappearance of the current peaks in *J–E* curves. Therefore, the S_{max}/E_{max} reaches an optimal value as high as ~ 616 pm/V at 50 °C, but then decreases to ~ 360 pm/V at 120 °C monotonously.

Figure 10a–c show the *P–E*, bipolar *S–E* and *S–P*^{2} curves of the BNST–0.08 ceramic at various temperatures. As mentioned above, this composition lies deeply in the ergodic relaxor state and exhibits a purely electrostrctive behavior

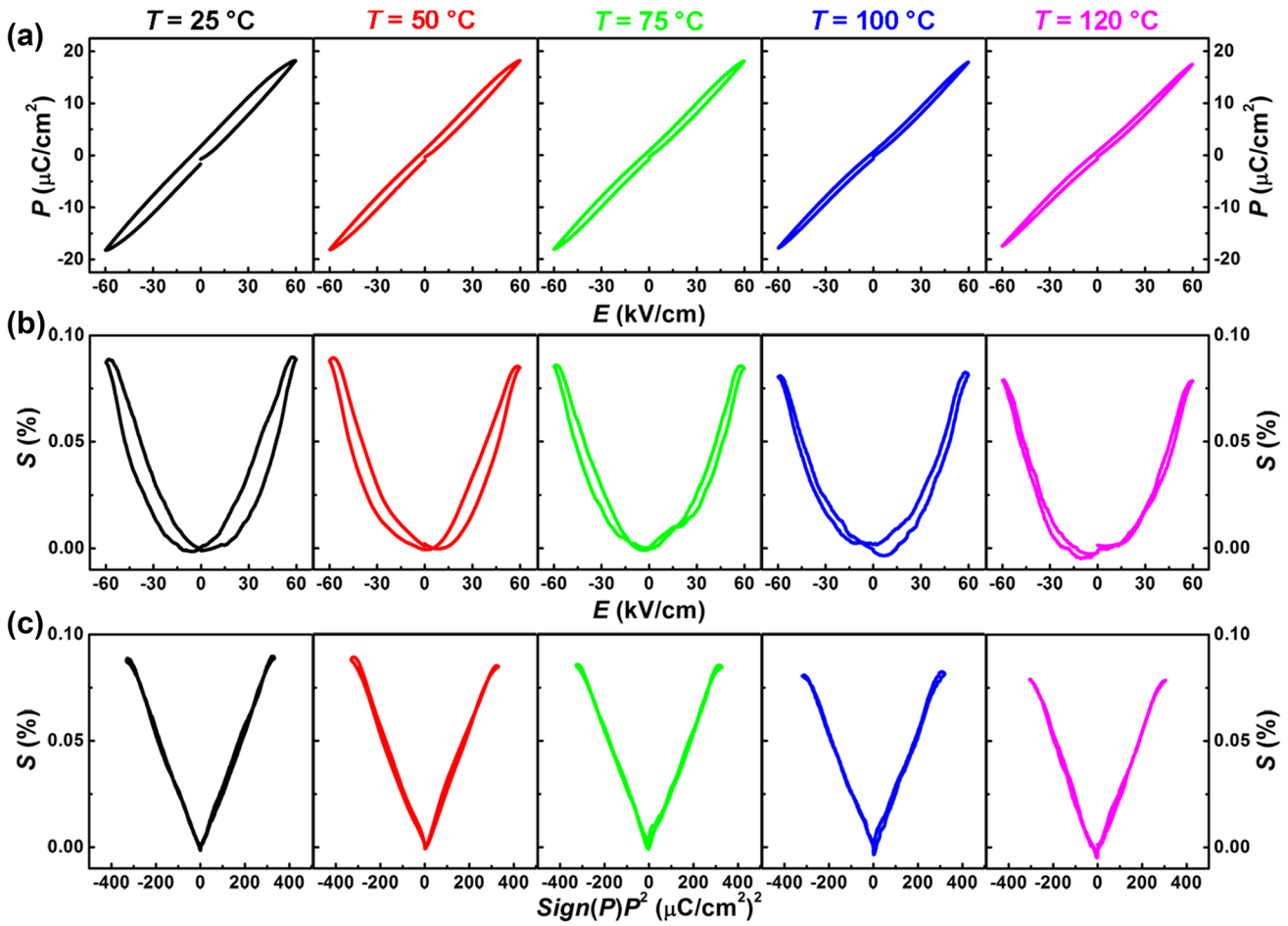

Fig. 10 **a** *P–E* loops, **b** bipolar *S–E* curves and **c** *S–P*^{2} profiles for the BNST–0.08LN electrostrictor at different temperatures

with a relative large Q_{33} of ~ 0.028 m^4/C^2 at room temperature. It was found that all the macroscopically electrical properties are highly stable against the change in temperature, analogous to other electrostrictors in literatures [18–20]. The P_m observed in the *P–E* loops and the S_{pos} reflected in the bipolar *S–E* curves keep nearly constant with the increased temperature from room temperature to 120 °C. As a result, the temperature-dependence of Q_{33} values measured at 60 kV/cm for this sample exhibits an excellent thermal stability with a little variation < 2% in the temperature range between room temperature and 120 °C, which should be benefited from the stable relaxor pseudo-cubic phase existed over a wide temperature range.

4 Conclusion

In summary, a series of the BNST–*x*LN (x = 0–0.08) piezoelectric ceramics were fabricated, and the influences of LN-doping on the phase structure and the electrical properties were systematically investigated. It was found that the addition of $LiNbO_3$ into the matrix material BNST has an effect to enhance the octahedral distortion of the crystal structure and improve the dielectric relaxation, leading to a phase transformation from the ordered ferroelectric phase to the ergodic relaxor state with dynamically active *PNR*s. At the critical composition x = 0.04, a large normalized strain (S_{max}/E_{max}) of ~ 600 pm/V was obtained at room temperature owing to the coexistence of the ferroelectric and ergodic relaxor phases, where the reversible transition between these two phases takes place under the external electric field as evidenced by the pinched *P–E* loop and the large hysteresis in the strain response. On the other hand, it is noted that the threshold field of the field-induced phase transition is enhanced remarkably by the further increase of LN content; consequently, the BNST–0.08LN ceramic exhibits a nearly pure electrostrictive behavior without the occurrence of domain switching. A Q_{33} value ~ 0.028 m^4/C^2 retains almost constant in the measured temperature range from 25 to 120 °C, indicating that this composition should be a promising lead-free electrostrictor.

Acknowledgements This work was financially supported by a grant from the State Key Program for Basic Research of China (2012CB619406), the National Natural Science Foundation of China (11174135, 51372111, and 11134004), and the Fundamental Research Funds for the Central Universities (1095021336 and 1092021307).

References

1. Y. Saito, H. Takao, T. Tani, T. Nonoyama, K. Takatori, T. Homma, T. Nagaya, M. Nakamura, Nature **432**, 84 (2004)
2. D. Damjanovic, N. Klein, J. Li, V. Porokhonskyy, Funct. Mater. Lett. **3**, 5 (2010)
3. J. Rödel, W. Jo, K.T.P. Seifert, E.M. Anton, T. Granzow, D. Damjanovic, J. Am. Ceram. Soc. **92**, 1153 (2009)
4. J. Rödel, K.G. Webber, R. Dittmer, W. Jo, M. Kimura, D. Damjanovic, J. Eur. Ceram. Soc. **35**, 1659 (2015)
5. S.-T. Zhang, A.B. Kounga, E. Aulbach, H. Ehrenberg, J. Rödel, Appl. Phys. Lett. **91**, 112906 (2007)
6. S.-T. Zhang, A.B. Kounga, E. Aulbach, T. Granzow, W. Jo, H.J. Ehrenberg, J. Rödel, J. Appl. Phys. **103**, 034107 (2008)
7. W. Jo, R. Dittmer, M. Acosta, J. Zang, C. Groh, E. Sapper, K. Wang, J. Rödel, J. Electroceram. **29**, 71 (2012)
8. W. Jo, T. Granzow, E. Aulbach, J. Rödel, D. Damjanovic, J. Appl. Phys. **105**, 094102 (2009)
9. R. Dittmer, D. Gobeljic, W. Jo, V.V. Shvartsman, D.C. Lupascu, J.L. Jones, J. Rödel, J. Appl. Phys. **115**, 084111 (2014)
10. M. Hinterstein, M. Knapp, M. Hoelzel, W. Jo, A. Cervellino, H. Ehrenberg, H. Fuess, J. Appl. Crystallogr. **43**, 1314 (2010)
11. J. Kling, X. Tan, W. Jo, H.J. Kleebe, H. Fuess, J. Rödel, J. Am. Ceram. Soc. **93**, 2452 (2010)
12. J.E. Daniels, W. Jo, J. Rödel, V. Honkimäki, J.L. Jones, Acta Mater. **58**, 2103–2111, (2010)
13. X.M. Liu, X.L. Tan, Adv. Mater. **28**, 574 (2016)
14. C.H. Hong, H.P. Kim, B.Y. Choi, H.S. Han, J.S. Son, C.W. Ahn, W. Jo, J. Materiomics **2**, 1 (2016)
15. G.H. Haertling, J. Am. Ceram. Soc. **82**, 797 (1999)
16. F. Li, L. Jin, Z. Xu, S. Zhang, Appl. Phys. Rev. **1**, 011103 (2014)
17. S.-T. Zhang, A.B. Kounga, J. Wook, C. Jamin, K. Seifert, T. Granzow, J. Rödel, D. Damjanovic, Adv. Mater. **21**, 4716 (2009)
18. S.-T. Zhang, F. Yan, B. Yang, W. Cao, Appl. Phys. Lett. **97**, 122901 (2010)
19. J. Shi, H. Fan, X. Liu, A.J. Bell, J. Am. Ceram. Soc. **97**, 848 (2014)
20. F. Wang, C. Jin, Q. Yao, W. Shi, J. Appl. Phys. **114**, 027004 (2013)
21. J. Li, F. Wang, X. Qin, M. Xu, W. Shi, Appl. Phys. A. **104**, 117 (2011)
22. H.-S. Han, W. Jo, J.-K. Kang, C.-W. Ahn, I.-W. Kim, K.-K. Ahn, J.-S. Lee, J. Appl. Phys. **113**, 154102 (2013)
23. T. Takenaka, K. Maruyama, K. Sakata, Jpn. J. Appl. Phys. **30**, 2236 (1991)
24. O. Elkechai, M. Manier, J.P. Mercurio, Phys. Status Solidi A **157**, 499 (1996)
25. Y. Hiruma, H. Nagata, T. Takenaka, J. Appl. Phys. **104**, 124106 (2008)
26. W. Krauss, D. Schütz, F.A. Mautner, A. Feteira, K. Reichmann, J. Eur. Ceram. Soc. **30**, 1827 (2010)
27. M. Acosta, W. Jo, J. Rödel, J. Am. Ceram. Soc. **97**, 1937 (2014)
28. W. Bai, L. Li, W. Li, B. Shen, J. Zhai, H. Chen, J. Am. Ceram. Soc. **97**, 3510 (2014)
29. X.Y. Tong, H.L. Li, J.J. Zhou, H. Liu, J.Z. Fang, Ceram. Int. **42**, 16153 (2016)
30. J.-H. Cho, J.-S. Park, S.-W. Kim, Y.-H. Jeong, J.-S. Yun, W.-I. Park, Y.-W. Hong, J.-H. Paik, J. Eur. Ceram. Soc. **37**, 3313 (2017)
31. W. Bai, L. Li, W. Wang, B. Shen, J. Zhai, Solid State Commun. **206**, 22 (2015)
32. J. Chen, Y. Wang, Y. Zhang, Y. Yang, R. Jin, J. Eur. Ceram. Soc. **37**, 2365 (2017)
33. J. Hao, W. Bai, W. Li, B. Shen, J. Zhai, J. Appl. Phys. **114**, 044103 (2013)
34. R.A. Malik, A. Hussain, A. Maqbool, A. Zaman, C.W. Ahn, J.U. Rahman, T.K. Song, W.J. Kim, M.H. Kim, J. Am. Ceram. Soc. **98**, 3842 (2015)
35. L. Wu, B. Shen, Q. Hu, J. Chen, Y. Wang, Y. Xia, J. Yin, Z. Liu, J. Am. Ceram. Soc. **100**, 4670 (2017)
36. A. Zaman, A. Hussain, R.A. Malik, A. Maqbool, S. Nahm, M.H. Kim, J. Phys. D **49**, 175301 (2016)
37. G. Xu, Z. Zhong, Y. Bing, Z.G. Ye, G. Shirane, Nat. Mater. **5**, 134 (2006)
38. J. Kreisel, A.M. Glazer, G. Jones, P.A. Thomas, L. Abello, G. Lucazeau, J. Phys.: Condens. Matter **12**, 3267 (2000)
39. G. Viola, H. Ning, X. Wei, M. Deluca, A. Adomkevicius, J. Khaliq, M.J. Reece, H. Yan, J. Appl. Phys. **114**, 014107 (2013)
40. D. Rout, K.S. Moon, S.J.L. Kang, I.W. Kim, J. Appl. Phys. **108**, 084102 (2010)
41. D. Schütz, M. Deluca, W. Krauss, A. Feteira, T. Jackson, K. Reichmann, Adv. Funct. Mater. **22**, 2285 (2012)
42. F. Li, G. Chen, X. Liu, J. Zhai, B. Shen, H. Zeng, S. Li, P. Li, K. Yang, H. Yan, J. Eur. Ceram. Soc. **37**, 4732 (2017)
43. W. Jo, S.S. Schaab, E. Sapper, L.A. Schmitt, H.J. Kleebe, A.J. Bell, J. Rödel, J. Appl. Phys. **110**, 074106 (2011)
44. X. Liu, J. Zhai, B. Shen, F. Li, Y. Zhang, P. Li, B. Liu, Curr. Appl. Phys. **17**, 774 (2017)
45. F. Li, R. Zuo, D. Zheng, L. Li, J. Am. Ceram. Soc. **98**, 811 (2015)
46. E. Sapper, N. Novak, W. Jo, T. Granzow, J. Rödel, J. Appl. Phys. **115**, 81 (2014)
47. F. Li, L. Jin, Z. Xu, D. Wang, S. Zhang, Appl. Phys. Lett. **102**, 152910 (2013)
48. W. Bai, D. Chen, P. Zheng, J. Zhang, B. Shen, J. Zhai, Z. Ji, Ceram. Inter. **43**, 3339 (2017)
49. R.A. Malik, A. Hussain, M. Acostad, J. Danielse, H.-S. Han, M.-H. Kim, J.-S. Lee, J. Eur. Ceram. Soc. **38**, 2511 (2018)